Journal of Constructional Steel Research 114 (2015) 51–65

Contents lists available at ScienceDirect

Journal of Constructional Steel Research

Seismic performance of controlled spine frames with energy-dissipating members

T. Takeuchi *, X. Chen *, R. Matsui *

Department of Architecture and Building Engineering, Tokyo Institute of Technology, Tokyo, Japan

ARTICLE INFO

Article history:
Received 11 May 2014
Received in revised form 20 June 2015
Accepted 3 July 2015
Available online xxxx

Keywords:
Spine system
Steel moment-resisting frame
Seismic performance
Vertical structural irregularity
Incremental dynamic analysis

ABSTRACT

Recently, various controlled rocking systems have been proposed in seismic design to prevent damage concentration and to achieve self-centering against a wide range of input ground motion intensities. However, several obstacles must be overcome before these systems can be applied to actual buildings; for example, the requirement for large, self-centering post-tensioned strands and special treatment at uplift column bases must be addressed. This paper proposes a non-uplifting spine frame system with energy-dissipating members without post-tensioned strands, its self-centering function is achieved by envelope elastic-moment frames. The system is applied to an actual building constructed in Japan. Conventional shear damper and uplifting rocking systems with post-tensioned strands developed in prior studies are also applied to the same building structures, and the performances of the three systems, including damage distribution, energy dissipation, self-centering, robustness against severe earthquakes, and irregular stiffness, are compared and discussed through numerical simulations based on practical design criteria.

1. Introduction

Steel moment-resisting frames are susceptible to large lateral displacements during severe earthquake ground motions and require special attention to limit damage to nonstructural elements. In the last few decades, buckling-restrained braced frames (BRBFs) have become increasingly popular, particularly in Japan and the USA, because of their superior seismic performance in limiting damage, maintaining functionality, and facilitating repair. Well-balanced buckling-restrained braces (BRBs) are required for ensuring the high seismic performance of BRBFs. This means that the yielding forces of the BRBs in each story are proportional to the story stiffness thus the BRBs yield at the same time in a first-mode response pattern. However, after the yield of the main frame under large seismic intensity, the low post-yield tangent stiffness of the braces may concentrate damage and residual drift in limited levels, even though brace capacities are relatively well balanced over the height of the structure [1].

Self-centering seismic resilient structural systems possessing the ability to limit residual drifts to negligible magnitudes have also been proposed. There are roughly three types of self-centering systems: (1) moment-resisting frames with post-tensioned (PT) beam-to-column connections and flexible floor systems that allow gaps to open between the beam-to-column connections [2]; (2) braced frames with self-centering braces or buckling-restrained braces (BRBs) that can return after loading to their initial length because of super-elastic pretensioned elements [3,4]; and (3) rocking systems that can self-center, relying on the restoring force of gravity, and PT elements [5–8].

Rocking motions may reduce damage to structures during ground motions. This behavior was observed as early as 1963, by Housner [9]. Clough and Huckelbridge [10] conducted some of the earliest rocking frame tests and compared them with a conventional pin-base frame. They found that the member force of the rocking frame was lower than that of the conventional frame. Priestley et al. [11] developed a simple method to evaluate the rocking response of structures via the displacement response spectra using the equivalent damping of the rocking system.

In the last decade, the rocking system has been used frequently in both retrofitting and new building design. Wada et al. [12] employed a pivoting spine concept in the seismic retrofitting of a concrete building in Japan and Janhunen et al. [13] employed a similar spine concept in the seismic retrofitting of a steel building in the USA. A concrete wall acts as the core of the rocking to redistribute the lateral forces and displacements without adding significant strength. Günay et al. [14] investigated the seismic performance of a brittle reinforced concrete frame, which was retrofitted with rocking infill walls, and proved its efficacy in reducing soft-story failure risks.

Eatherton et al. [15–18] studied an uplifting rocking frame system with PT strands that provide self-centering resistance. Steel butterfly-shaped fuses and BRBs were employed as replaceable energy-dissipation members. Midorikawa et al. [5,19] conducted shaking-

* Corresponding authors at: Tokyo Institute of Technology, M1-29, 2-12-1 Ookayama, Meguro-ku, Tokyo 152-8550, Japan.
E-mail addresses: ttoru@arch.titech.ac.jp (T. Takeuchi), chen.x.ad@m.titech.ac.jp (X. Chen), matsui.r.aa@m.titech.ac.jp (R. Matsui).

http://dx.doi.org/10.1016/j.jcsr.2015.07.002
0143-974X/

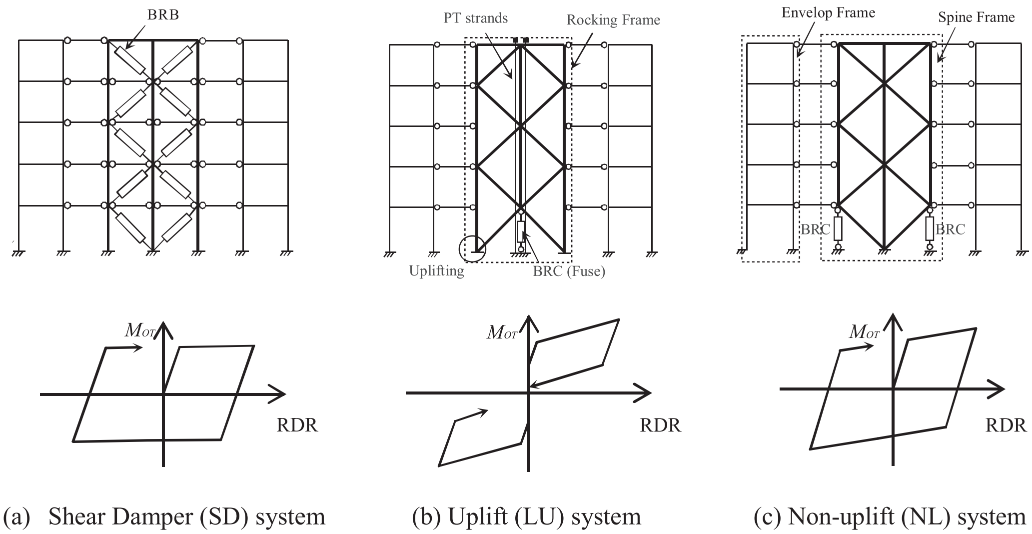

Fig. 1. Concept of element configuration and hysteretic curves of the three structural systems.

table tests of a half-scale three-story rocking frame after installing yielding plates at the bases of columns to dissipate energy. Wada et al. [7] used a similar concept at the connections of columns in the middle story of a slender, tall frame. Tremblay et al. [8] proposed a braced steel frame with viscous dampers vertically equipped between the column bases and the foundations.

Ikenaga et al. [20] developed a column base consisting of PT bars and steel plate dampers. Takamatsu et al. [21] proposed a column base with anchor bolts that dissipate energy by elongation. Takeuchi and Suzuki [22] used buckling-restrained columns (BRCs) at the bases of truss frames to concentrate major damage into the BRCs and prevent collapses caused by the buckling of members in the main structure.

As mentioned above, effective and economical structural systems eliminating damage concentration and residual drift after large earthquakes are needed and have been frequently investigated; however, applications to actual buildings are not yet popular. This is mainly because several obstacles must be overcome, such as the need for large, self-centering PT strands and special treatment at uplift column bases. To eliminate these difficulties, in this paper, we investigate a non-uplifting spine frame system without PT strands whose self-centering function is achieved by envelope elastic-moment frames. The proposed system was tested by applying it to an actual building structure under construction, and its performance is compared with a conventional BRBF and controlled rocking frame with PT strands.

Fig. 2. Materials Research Center for Element Strategy (MCES), Tokyo Tech.

2. Design and modeling of structural systems

2.1. Concepts of non-uplifting spine frame systems

Fig. 1 shows the three structural systems examined in this paper and the relationship between the overturning moment (M_{OT}) and roof drift ratio (RDR) of the proposed system compared with the two existing systems. A conventional frame with shear dampers as BRBs (hereafter referred to as the SD system; Fig. 1(a)) generally shows excellent performance as long as the main structure is well balanced in terms of stiffness and remains elastic. However, for unbalanced and elasto-plastic ranges of the main frames, damage concentration at weak stories and residual deformations are expected after an earthquake. To decrease such risks, a controlled uplifting rocking frame system (hereafter referred to as the LU system; Fig. 1(b)) was proposed [24], in which a rocking spine frame was introduced to distribute damage uniformly throughout the stories and PT strands were introduced to achieve self-centering functions. However, the prestressed forces required for PT strands are higher than the expected residual forces of energy-dissipation fuses (BRCs), which often reach to several thousand kN in actual projects, and the details of uplifting systems tend to be complicated. To overcome these problems, a non-uplifting spine frame system

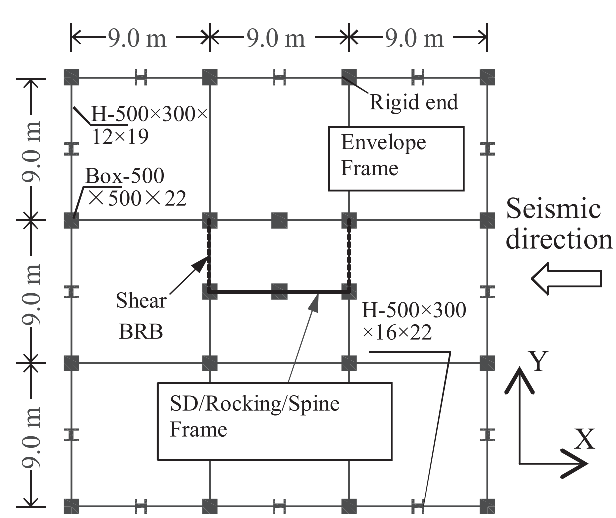

Fig. 3. Plan of the building.

Table 1
Dimensions, gravity load, and mass distribution of the models.

	Story height (m)	Span of beam (m)	Gravity load (kN/m^2)	Mass (ton)
Roof	–	4.5	11.3	788
Second–fifth stories	4.0	4.5	7.65	495
First story	4.2	4.5	–	–
Total	20.2	27	30,500	27,000

Table 3
Cross-sectional areas and yielding forces of BRBs in SD model.

Story	Cross-sectional area, A_{BRBi} (mm^2)	Yielding force, F_{y_BRBi} (kN)
5	4300	970
4	5900	1330
3	7100	1600
2	8000	1800
1	8700	1960

(hereafter referred to as the NL system; Fig. 1(c)) is proposed in this paper. The proposed system comprises steel braced frames and replaceable energy-dissipating fuses (BRCs) without PT strands; its self-centering functions are achieved by envelope elastic-moment frames. Unlike those in the LU system, the columns in the NL system are replaced by BRCs and are fixed to the foundation. Under earthquakes exceeding specific levels, plastic hinges activate at the bottom, and the braced spine frame rocks around the center. During rocking, the rocking frames remain elastic while the energy is dissipated by the plastic deformation of replaceable fuses. After the shaking, the restoring forces from the envelope moment-resisting frames play a role in self-centering the system. The rocking braced frame acts as the spine element of the entire structure to prevent damage concentration, even when the envelope frame includes weak stories. With proper design, the self-centering capacity can be ensured to achieve immediate occupancy of the building.

2.2. Building models

The proposed structural system was applied to an actual building under construction in the Tokyo Institute of Technology Suzukakedai campus. Figs. 2 and 3 illustrate the perspective view and plan of the building, respectively. Although we intended placing spine frames in a crucifix-shaped configuration in the core of the plan; because of the architectural requirements, only a groove-shaped space at the core was available. As a result, we employ the NL frames and SD frames in each direction other than employing both NL frames. In the following, the performance in the spine frame direction is mainly discussed, followed by hybrid actions under angled seismic inputs.

The story height of the building is typically 4 m at regular stories; the first story is 4.2 m high. The plan dimensions are 27 m × 27 m: 4.5 m × 4.5 m bays for the external frames, and 9.0 m × 9.0 m bays for the internal frames. The braced bay is located in the middle of the building. To evaluate the performance of the proposed structural system, a model of the same envelope steel moment-resisting frame (SMRF) with the SD system, a model of the LU system, and a model of the proposed NL system were designed with the same configuration and earthquake input. Although the structure was designed with a rocking (BRB) frame in the X-direction and shear BRBs in the Y-direction, the effects of these shear BRBs in the Y-direction are not considered in this paper, so that the performances of the three systems can be compared in the X-direction.

The seismic performance of the building was evaluated at two limit states: (1) damage initiation state and (2) life-safety limit state. These states correspond to a hazard of 63.6% and 10% probability of exceedance in a 50-year period. The standard shear force coefficients, C_0, were set to 0.2 and 1.0 for the two seismic levels, and the maximum story drift ratios were controlled at less than 0.5% and 1%, respectively. The second limit state is close to the design-basis earthquake level (DBE level) in California. The envelope structural framework was designed to remain elastic, and most of the input seismic energy was absorbed by the energy-dissipation members. The detailed design procedure is shown in Appendix A. Table 1 lists the dimensions of the building, the gravity load, and the mass distribution. Table 2 lists the sizes and the materials of typical members.

The SD model was designed with the initial stiffness and yielding force of BRBs in each story in proportion to the *Ai* distribution, which is the suggested lateral force distribution related with the fundamental period in Japan seismic code. A detailed calculation method is described in Appendix A. The cross sections and yielding forces of BRBs in each story are listed in Table 3.

The LU model with BRCs and PT strands was designed by replacing BRBs in the SD model with a rocking spine with a stiff H-shaped steel truss, which remains mostly elastic in the second limit state. The yielding force of the BRC and the prestress force of the PT strands were selected by determining an initial yielding overturning resistance of the rocking frame that was equal to the yielding overturning moment of the SD model. The overturning moment of the SD model was 46,000 kNm. Eq. (5) expresses the initial yielding overturning moment of the LU rocking frame.

$$M_{OT} = \left(G_{rf} + F_{PT} + F_y^{BRC}\right) \cdot \frac{b_{rf}}{2} \tag{5}$$

where M_{OT} is the overturning moment; G_{rf} is the dead load of the rocking frame; F_{PT} is the axial force of the PT strands when the BRC yields; F_y^{BRC} is the yielding force of the BRC; and b_{rf} is the width of the rocking frame. The dead load, G_{rf}, was 3390 kN. The total cross-sectional area of the PT strands was 8300 mm^2, and the initial tension force was 1860 kN, which is 11.3% of the yielding force of the PT strands. The cross-sectional area and the yielding force of the BRC were 13,900 mm^2 and 4970 kN, respectively. The sum of the dead load and the initial tension force, at 5250 kN, was larger than the yielding force of the BRC, thus ensuring the self-centering system of the rocking frame.

The proposed NL model employs the same rocking spine frame as that in the LU model, and energy-dissipation fuses (BRCs) are distributed at the bases of side columns of the spine frame. The braces and central column are rigidly connected to the foundation, and plastic hinges activate at large rocking drift. The BRCs are located along the lines of the side columns to maximize their energy-dissipation performance. The yielding force of the BRCs was selected by determining an initial yielding overturning resistance of the spine frame that was equal to that of the LU model. Eq. (6) expresses the initial yielding overturning moment of the spine frame of the NL model.

Table 2
Sizes and materials of typical members.

Structural members	Size (mm)	Material	M_p (kNm)
Beams in SMRF	H-500 × 300 × 12 × 19	SN400B	870
Columns in SMRF	Box-500 × 500 × 19	SN490B	2360
Columns in SD/rocking/spine frame	Box-550 × 550 × 25	SN490B	3700
Diagonals in rocking/spine frame	H-600 × 550 × 25 × 25	SN490B	3374

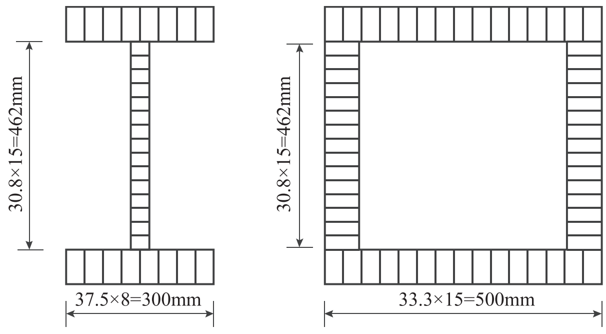

Fig. 4. Fiber discretization of a typical beam and a typical column.

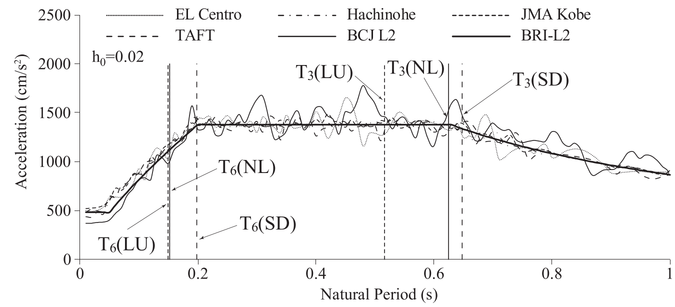

Fig. 6. Acceleration spectra of normalized input ground motions ($h_0 = 0.02$).

$$M_{OT} = F_y^{BRC} b_{rf} \tag{6}$$

where M_{OT} is the overturning moment of the spine frame; F_y^{BRC} is the yielding axial force of the BRC on one side; and b_{rf} is the width of the spine frame. The cross-sectional area and the yielding force of the BRCs were 13,900 mm^2 and 4500 kN, respectively.

The spine frame is connected to the outer moment frames through pin-ended beams. These beams are designed with sufficient stiffness to transmit horizontal force without extensive axial deformation, but they do not restrain the vertical displacement of the rocking frames.

2.3. Numerical model

Detailed three-dimensional numerical models of the building were developed in the OpenSEES computational environment [23]. Centerline dimension models, which ignore the effects of panel zones and gusset plates, were employed for all models. A model with centerline dimensions normally overestimates the maximum force of the elements; however, it has no influence on our comparison of the three structural systems [24].

Beams, columns in the main frame, and braces in the rocking frame were divided into four elements. Each element consisted of an iterative force-based beam element with three Gauss–Lobatto integration points and fiber discretization of the cross-section. The dimension of each fiber is approximately 35 mm × 20 mm. Fig. 4 shows the fiber discretization of a typical beam and a typical column. With this approach, the element responses were derived by integrating the uniaxial stress–strain relationship of each fiber, which also accounted for the coupling effect between axial force and bending moment. Additionally, the plasticity developing along the depth of the sections and length of the elements was encompassed for these structural members. Shear deformation and global or local buckling of members were not taken into account. The BRB (BRC) and PT strands were modeled as pin-ended truss members. All beam-to-column connections in the SMRF were modeled as rigid connections. P-Delta effects were included in the transformation of the column and brace elements. A rigid floor was assumed, to ensure that the rocking frame worked together with the outer frame. All uniaxial materials were assumed to have bilinear stress–strain relations with a kinematic hardening rule. The yielding strength and strain-hardening ratio assigned to BRBs are set as 275.5 MPa and 0.4% respectively. The yielding strength of other structural members is 357.5 MPa or 258.5 MPa. Their strain-hardening ratio is set as 1.0%. Rayleigh damping with 0.02 critical damping ratio matching at the third and sixth modes was implemented in the model.

In the modeling of BRBs/BRCs, we adopted equivalent elastic modulus and equivalent strain hardening ratio in order to consider that contribution of the higher axial stiffness of the elastic portions of the same member. Detailed equations are listed in Appendix B.

3. Seismic performance of the three structural systems

3.1. Static analysis

Pushover analyses were carried out under the external lateral force on each floor proportional to the equivalent elastic lateral force obtained by the first vibration mode response (*Ai* distribution) for each model. The results are shown in Fig. 5. The yielding overturning moments of the three models were calibrated at approximately 46,000 kNm. The LU rocking frame featured a larger hardening ratio than the other two models because the PT strands remained elastic during loading, but the difference was smaller in the responses of the entire structures.

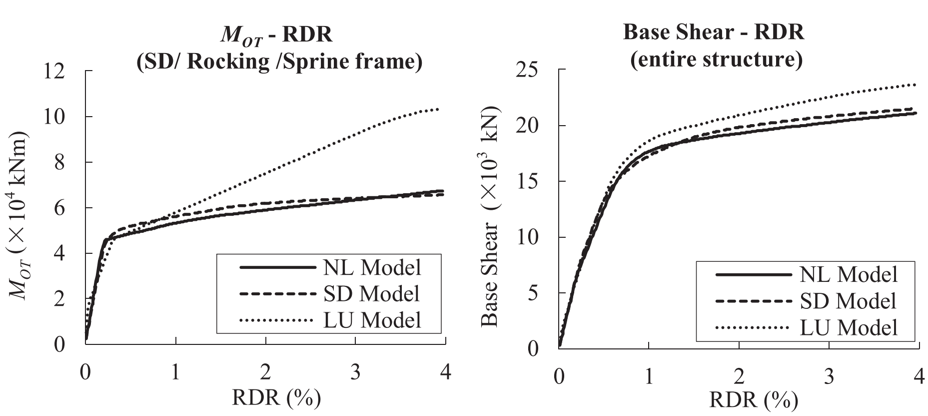

Fig. 5. Pushover analysis results of the three models.

Table 4
Elastic natural periods (unit: s).

Mode	Third	Sixth
NL model	0.630	0.152
LU model	0.516	0.149
SD model	0.646	0.198

3.2. Selection of ground motions

The ground motions used herein included one artificial wave (BCJ-L2) and four observed waves: El Centro NS (1940), JMA Kobe NS (1995), TAFT EW (1925), and Hachinohe NS (1968). The duration of BCJ-L2 was 120 s and the duration of the four observed waves was 30 s for each wave. The response acceleration spectra of the four recorded ground motions were scaled to follow the design spectra averaged for the life-safety limit state (BRI-L2) in Japan, as shown in Fig. 6.

For all three models, we examined the response of the first and fourth modes to translational deformation in the Y-direction in Fig. 3, the response of the second and fifth modes to rotation in the plan, and the response of the third and sixth modes to translational deformation in the X-direction. The elastic natural periods of the third and sixth modes of each model are shown in Table 4. The third mode period of the LU model is larger than the other two models because the period is calculated before the spine frame bottom uplifting in the LU model. In this stage, the stiffness of the LU model is larger than the other two models because of the high-stiffness PT strands. However, once uplifting occurred, the stiffness of the LU model reduces to be slightly lower than the other two models. The overall stiffness of the LU model after uplifting is similar with the other two models, which can be seen in Fig. 5. The uncoupled torsional-to lateral frequency ratios of the Model SD, LU, and NL are 0.79, 0.65, and 0.81, respectively.

3.3. Time-history analysis

3.3.1. Interstory drift

Fig. 7 shows the overturning moment and RDR loops of the three models, determined from time-history analysis. The self-centering flag-shaped behavior of the LU model was confirmed in the response during numerical simulation. Fig. 8 shows the story drift ratio (SDR) time-history response of the second story under Hachinohe ground motion input, including the peak responses. The maximum values of the three models occurred at approximately the same point in time. The maximum SDRs of each story in the three models are shown in Fig. 9. Among all 15 results, only the SDR of the second-story drift in the SD model under Hachinohe ground motion input exceeded 1%.

The SD model had a strong tendency to concentrate deformation in the second story. In contrast, the LU and NL models distributed a more uniform SDR owing to their spine mechanisms. To better understand

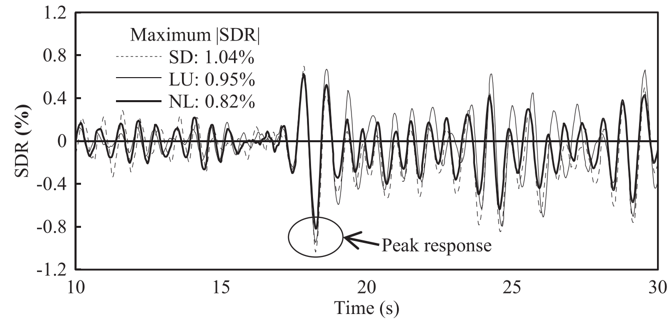

Fig. 8. SDR time-history response of second story (Hachinohe NS).

the effectiveness of spine frames in reducing deformation concentration, the ratio of maximum SDR to RDR is used to express the story drift concentration factor (DCF) [12]. As shown in Fig. 10, under all five ground motions, the proposed NL model exhibited the smallest DCF, the DCF of the LU model was higher, and the SD model displayed the highest DCF. Among all three models, the NL model exhibited the smallest peak story drift and the smallest DCF.

3.3.2. Residual story drift

The residual story drift is calculated after adding 60 s of analysis with zero ground accelerations. At the end of the analysis the model almost stopped moving. The residual story drift is taken as the drift when the velocity reaches zero for the last time. Fig. 11 shows the residual story drift ratio (ReSDR) of each story in all three models. All ReSDR values were less than 0.12%, and less than 0.05% in the LU and NL models. Fig. 12 shows the maximum base shear force of each model. The base shear forces were close to the yielding strength obtained from the pushover analysis, which means that the main frames were almost elastic.

The maximum shear force of the LU model tended to be greater than that of the SD model; however, the ReSDR of the LU model was smaller than or similar to that of the SD model. Unlike the case of the LU model, the maximum shear force of the NL spine system was identical to that of the SD model, whereas the ReSDR of the NL model was smaller than that of the SD model in all cases. This suggests that the elastic reaction forces from the envelope frame of the NL spine system were sufficiently large to overcome the residual axial force of the BRCs. This indicates that the proposed NL spine system possesses excellent resilience capacity when the envelope SMRF is elastic or yields slightly.

3.3.3. Energy dissipation

The input energy is dissipated by the system damping mechanism and the cumulative plastic deformation. The kinetic energy and elastic strain energy were negligible at the end of the analysis compared with the damping and cumulative plastic strain energy (CPE). The CPEs of the five ground motion inputs for the SD, LU, and NL models were

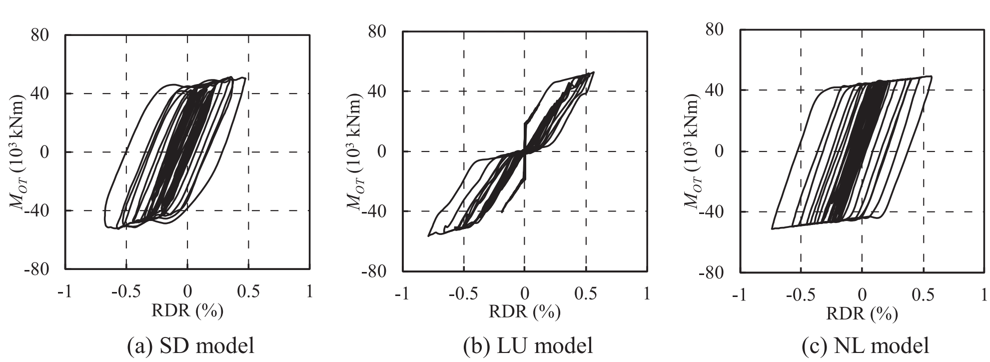

Fig. 7. Overturning moment and roof drift ratio hysteresis loops (Hachinohe NS).

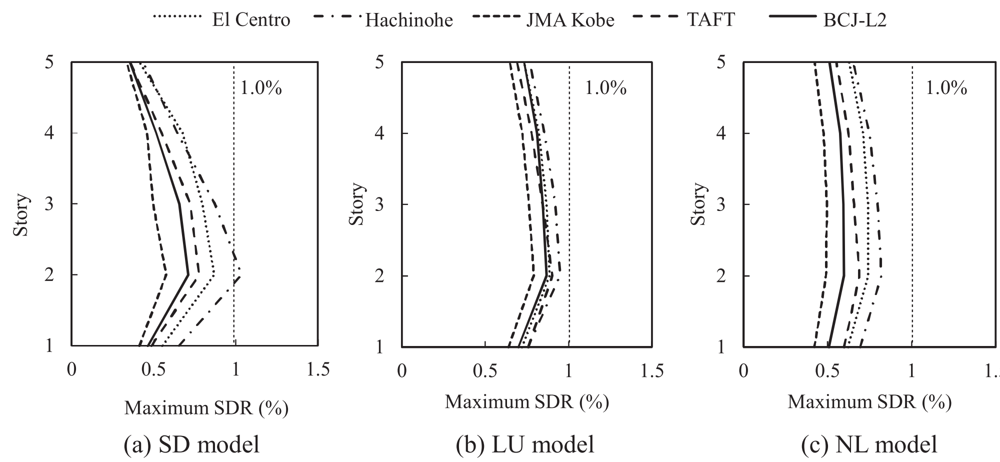

Fig. 9. Maximum story drift ratio of each story in SD, LU, and NL models.

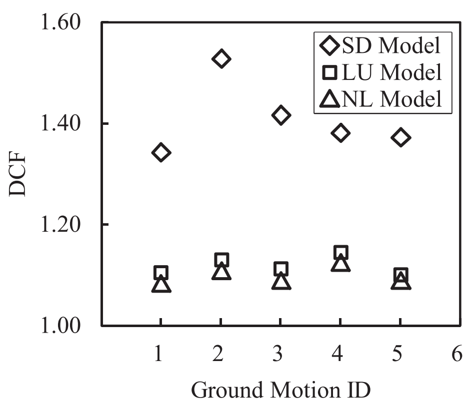

Fig. 10. Drift concentration factors of SD, LU, and NL models (ground motion IDs: 1. El Centro; 2. Hachinohe; 3. JMA Kobe; 4. TAFT; 5. BCJ-L2; these are the same in the following figures).

25 MN·m, 14 MN·m, and 25 MN·m, respectively; the damping energy values were 14 MN·m, 24 MN·m, and 15 MN·m, respectively; and the total input energy values were 39 MN·m, 38 MN·m, and 40 MN·m, respectively. The input energy values of the three models were close to each other. Conversely, the damping energy of the LU model was larger than that of the SD and NL models. A larger velocity response was also observed in the LU model than that in the SD and NL models. This indicates that the flag-shaped hysteretic response of the LU model had a lower capacity for energy dissipation. As a result, the amount of input energy that was converted into kinetic energy and absorbed by the damping mechanism in the LU model was larger than that in the SD and NL models.

In Fig. 13, the non-hatched areas in the bar chart represent the CPE of the BRBs or BRCs, and the hatched areas represent the envelope frames. The numbers above each bar denote the percentage of CPE of the BRBs or BRCs in the total CPE of the structures. In the proposed NL spine system, the earthquake input energy was greatly dissipated by the two BRCs at the bottom of the spine frame. The percentages of CPE of the BRCs in the total CPE of the structure ranged from 90.74% to 99.91%. Similar to the NL spine system, the BRBs in the SD system dissipated more than 85% of the CPE. For the LU rocking system, the main frame dissipated up to 60% of the total CPE, which was greater than the energy dissipated by the BRC.

Because the duration of the BCJ-L2 ground motion was longer than that of the four observed ground motions, the CPE of the main frame was compared among only the four observed waves. The proposed NL model had the best distribution of energy dissipation and the lowest CPE of the envelope frame, as illustrated in Fig. 14. This model dissipated energy through the beams from the first floor to the fourth floor; however, all the members in the spine frame and columns remained elastic. The largest amount of CPE in one story of the envelope frame in the NL model was 125.12 kNm. The envelope frame in the SD model dissipated the most energy in the second and third floors, as shown in Fig. 14, which indicates that damage was concentrated at those locations. The largest amount of CPE in one story of the SD model was 246.46 kNm. The main frame in the LU model dissipated the largest amount of energy

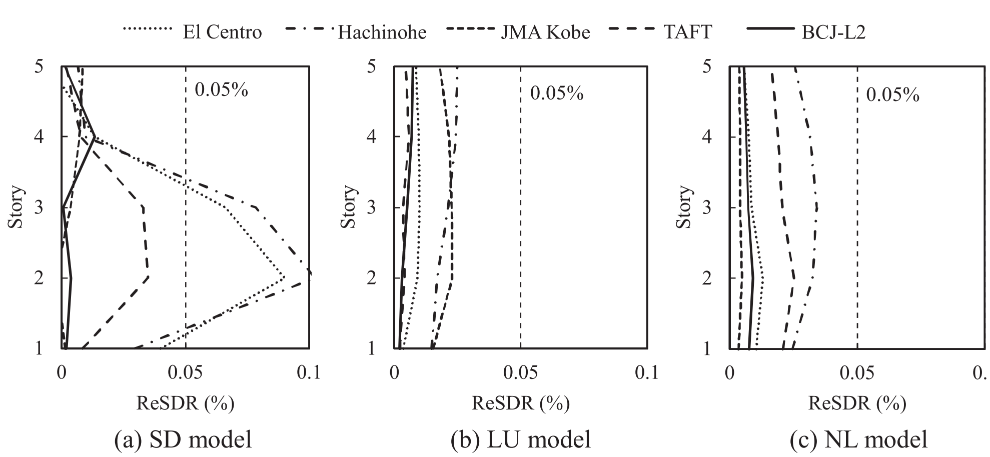

Fig. 11. Residual story drift ratio of each story in SD, LU, and NL models.

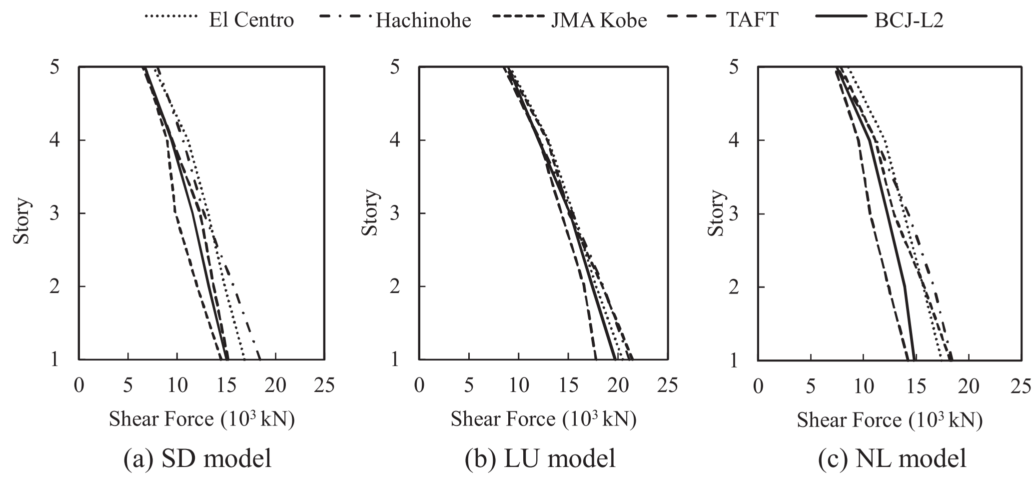

Fig. 12. Maximum shear force of each story in SD, LU, and NL models.

compared with the other two systems. The peak value of CPE in one story of the LU model was 677.90 kNm. The main frame of the proposed NL model suffered the least damage among all three models.

3.4. Incremental dynamic analysis

The LU rocking frame is expected to avoid damage concentration and eliminate permanent story drifts of the structures. However, its robustness remains unclear under unexpectedly strong earthquakes, which may lead to yielding of the PT strands. Incremental dynamic analysis (IDA) [25] was conducted to compare the seismic safety of the three structural systems, focusing particularly on the ultimate state of the LU rocking system after yielding of the PT strands and the performance of the NL spine system subjected to the same earthquake level.

The intensity measure (IM) was the peak ground acceleration (PGA). The damage measure (DM) was the maximum story drift ratio. The selected ground motions were scaled up until the maximum SDR reached 10% or until the PGA reached 6 g (60 m/s^2). The IDA curves of the three models are compared in Fig. 15.

Generally, for the SD model, the softening of the IDA curves was more significant than that of the NL and LU models, although the strength deterioration was not considered in the models. Yielding of the PT strands occurred when the maximum SDR was approximately 5%. Only under the Hachinohe ground motion input, after the PT strands yielded, the maximum SDR in the LU frame grew significantly faster than the NL frame with increased earthquake input intensity. Under other earthquake inputs, the differences were not significant between the IDA curves of the LU and NL models immediately after the PT strands yielded; generally, the maximum SDR of the SD model exceeded those of the NL and LU models with the same ground motion intensities.

4. Seismic performance with single-story irregular configuration

Building structures with vertically unbalanced strength distributions are commonly seen in modern urban areas, primarily because of architectural constraints. According to previous studies, the strength, stiffness, and mass irregularity significantly degrade the seismic behavior of these structures [26,27]. Special attention is necessary in the design of such irregular buildings. The proposed NL spine frame system is expected to distribute damage throughout the structure under a certain level, even for irregular building configurations. To evaluate the structural response of the three systems with vertical irregularities, the models in previous sections were modified by degrading both the stiffness and strength of all columns in a certain story of the moment-resisting frame. Two groups of irregular models were created, first-story irregular model and second-story irregular models, corresponding to irregularity in the first and second stories. Fig. 16 shows the shear force and SDR relationship of each story in the irregular models compared with regular models. The curves were determined through pushover analysis with equivalent horizontal force following *Ai* distribution. For all the SD, LU, and NL models, the degradation of the first-story columns caused obvious degradation in the strength of every story, particularly for the first story of the SD model. The degradation of the second-story columns significantly decreased the stiffness and strength of the second story in the SD model; however, it had a negligible influence on the stiffness and strength of every story in the LU and NL models.

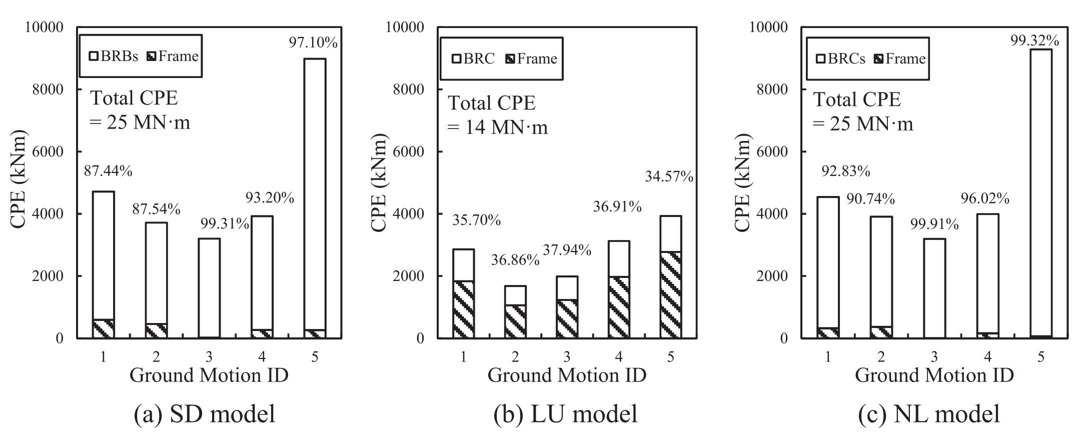

Fig. 13. Energy absorbed by energy-dissipating devices and envelope frames.

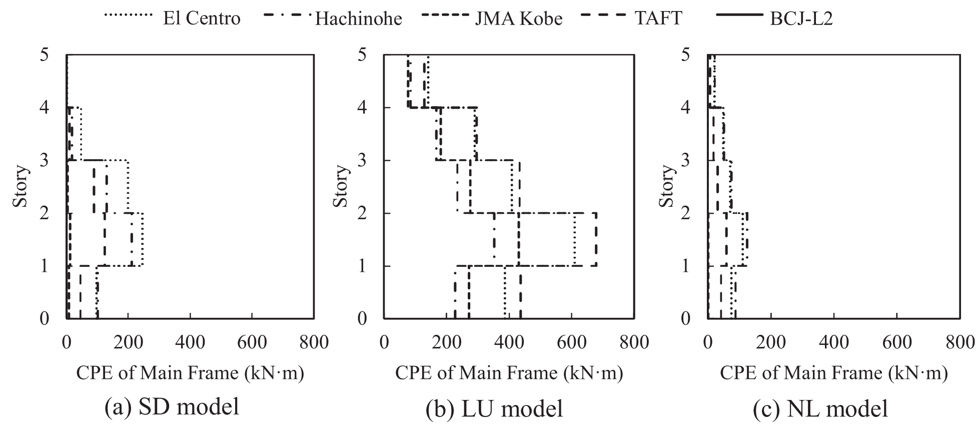

Fig. 14. Distribution of cumulative plastic strain energy (CPE) in each story of the envelope frame.

4.1. Interstory drift

The maximum SDR of each story in the irregular models is shown in Fig. 17. Among the first-story irregular models, the maximum first-story SDR of the SD model was approximately 1.2%, and the maximum SDRs of the LU and NL models were approximately 1%. Among the second-story irregular models, the maximum second-story SDR of the SD model was approximately 1.5%, that of the LU model was again approximately 1%, and that of the proposed NL model was the smallest among the three models.

The DCFs of the irregular models are shown in Fig. 18. It is clear that even for the irregular models, the LU and NL models controlled a more uniform story drift distribution over the height of the building than the SD model did. Similar to the results of the regular models, the proposed NL model had the smallest SDR among the three models, and its DCF was close to that of the LU model.

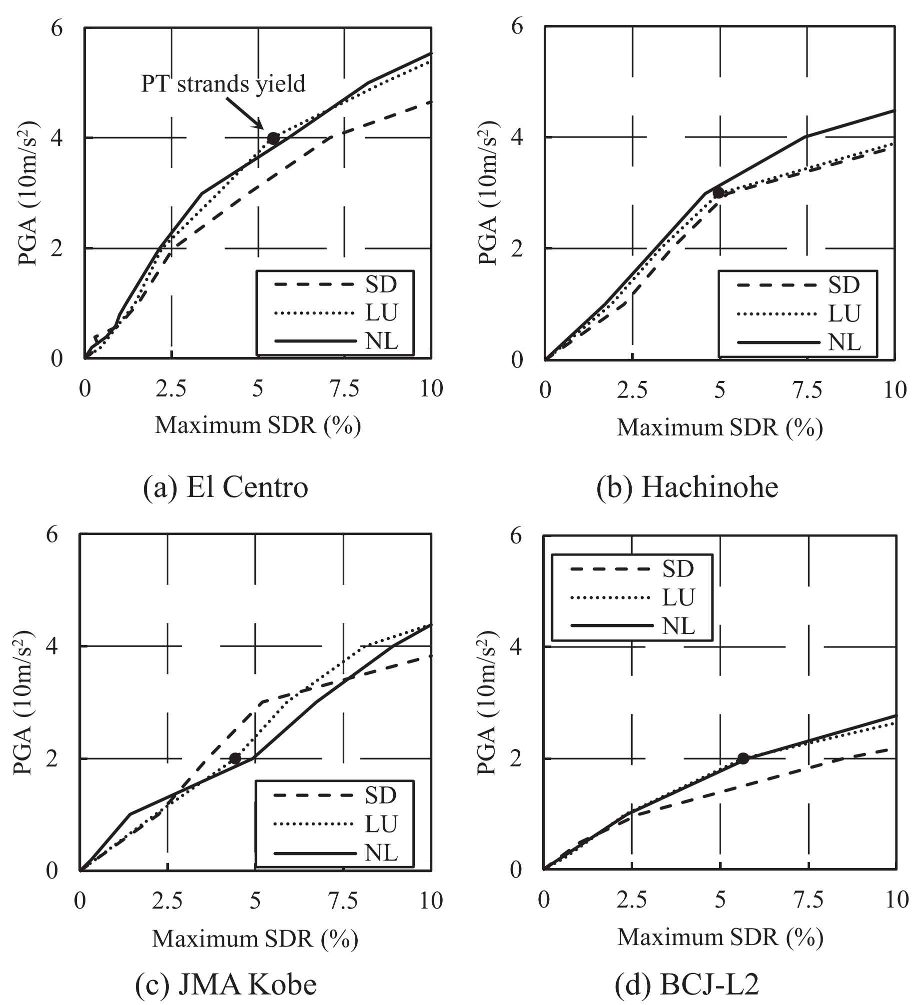

Fig. 15. Incremental dynamic analysis curves of the SD, LU, and NL models.

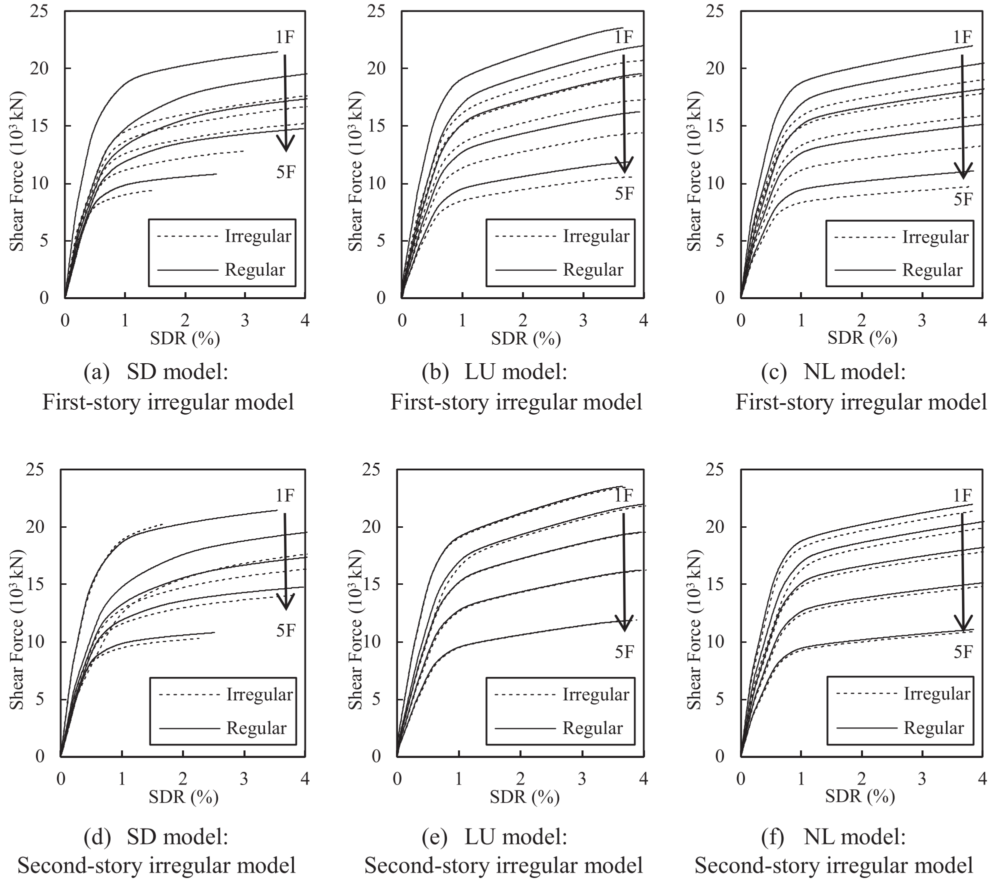

Fig. 16. Relationship between shear force and story drift ratio (SDR) in regular and irregular models.

4.2. Residual story drift

Fig. 19 shows the ReSDR of each story in all irregular models. Among the first-story irregular models, the maximum ReSDR of the SD model was approximately 0.25%; conversely, the maximum ReSDRs of the LU and NL models were approximately 0.05%. For the second-story irregular models, the maximum ReSDR of the SD model was also approximately 0.25%, and those of the LU and NL models were even smaller than those of the first-story irregular models.

4.3. Incremental dynamic analysis

IDA using the same IM (PGA) and DM (maximum SDR) was also conducted for the irregular models. The IDA curves of the first-story irregular models are shown in Fig. 20, and those of the second-story irregular models are shown in Fig. 21.

Among the first-story irregular models, the bottom diagonal member in the rocking frame of the LU model yielded when the PGA of input ground motions was 0.6–1.0 g (6–10 m/s^2 PGA). After the diagonals yielded, the maximum SDR of the LU model increased rapidly as the earthquake input intensity increased; this value was much weaker than that in the NL model, but was similar to that of the SD model. This is because the yielded diagonals could not maintain the rocking mechanism, so the upper stories deformed by sliding from the first floor. Because of this phenomenon, the PT strands did not yield when the maximum SDR was approximately 5%, but yielded when the maximum SDR was larger than 9%. The degradation of the bottom diagonal is another factor that influences the robustness of the LU model. For the first-story irregular NL model, in comparison, the maximum SDR at the same input intensity increased compared with the regular models, but the slope of its IDA curves decreased much more slowly than those of the LU and SD models, which indicates a more stable seismic behavior.

For the second-story irregular models, the SD model exhibited similar IDA curves to the first-story irregular SD model; whereas the LU and NL models both exhibited similar IDA curves to their regular models. The PT strands yielded when the maximum SDR was approximately 5%, and the bottom braces yielded after the PT strands yielded. Before the yielding of the bottom diagonals, the IDA curves of the LU model were entirely coincident with the curves of the NL model. However, after the bottom diagonals yielded, the slope of the IDA curves in the LU model decreased more than that of the NL model, although this result is not shown here. Thus, the proposed NL spine system showed the best damage distribution performance and self-centering performance among all cases even without PT strands.

5. Seismic performance of structures with hybrid systems

The previous sections investigated single-directional seismic performance of three structures employing the SD, LU, and NL frames respectively. In actual structural design, two directional seismic performance need to be considered. Employing NL frames and SD frames in each direction is more practical than employing both NL frames in terms of architectural requirements. The NL model studied in previous sections was modified by adding two perpendicular SD frames connected to the side columns of its NL frame, as shown in Fig. 22. Time history analysis with design level earthquake input in different directions was conducted. Cumulative strain energy dissipated by BRBs in the SD frames and BRCs in the NL frame was compared in Fig. 23.

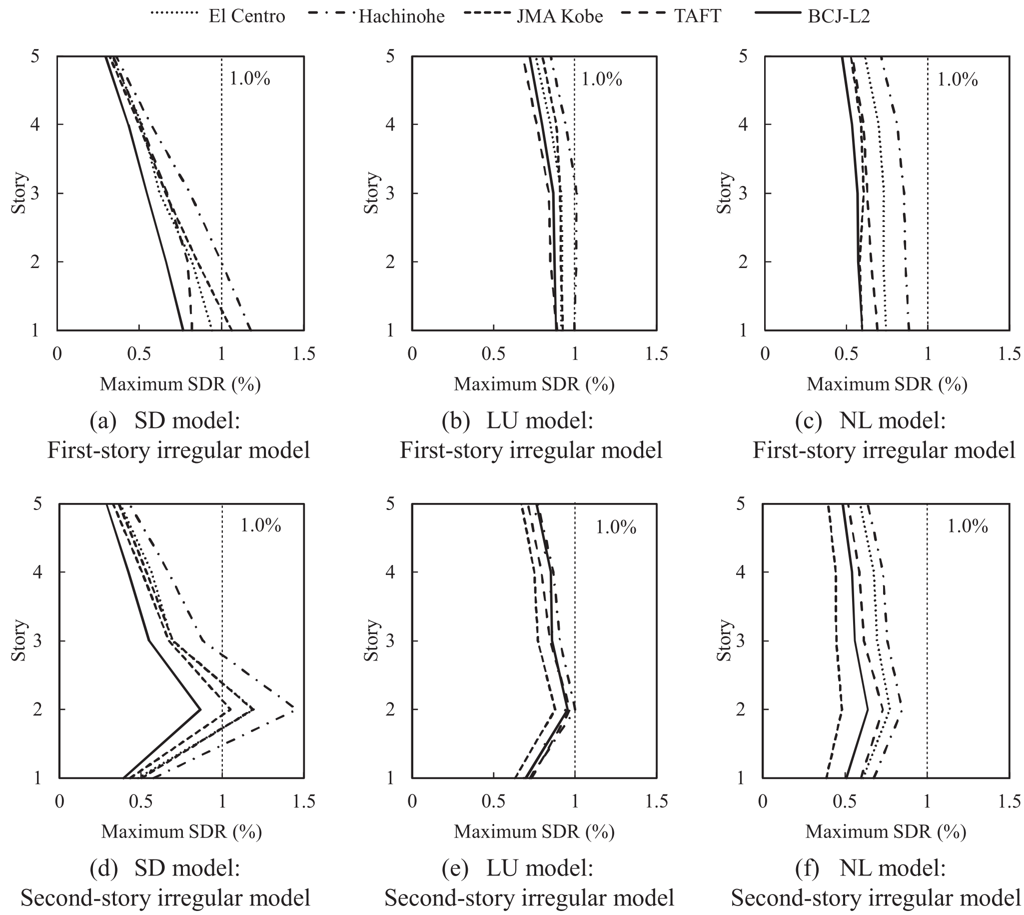

Fig. 17. Maximum story drift ratio (SDR) of each story in irregular models.

When the seismic input was in X direction, not only BRCs in X direction but also BRBs in Y direction dissipated energy. That's because the vertical displacement of the NL frame caused axial deformation of BRBs, which were directly connected with the NL frame. When the seismic input was in Y direction, only BRBs in Y direction dissipated energy, without any interaction with the NL frame. When the seismic input was in XY direction, the BRCs and BRBs both dissipated energy. However, the amount of energy was not the average of the amount obtained from X direction input and Y direction input, which indicated that the structural behavior in XY direction was not a simple superposition of its behavior in X direction and Y direction.

6. Conclusions

A non-uplifting spine system without PT strands and with elastic envelope frames was proposed. Its seismic performance was compared with a conventional shear damper system and a controlled uplifting rocking system through application to an actual building prototype under construction. The following conclusions were drawn from this study.

(1) For the regular models with balanced vertical strength distributions subjected to a design-level earthquake, the proposed NL

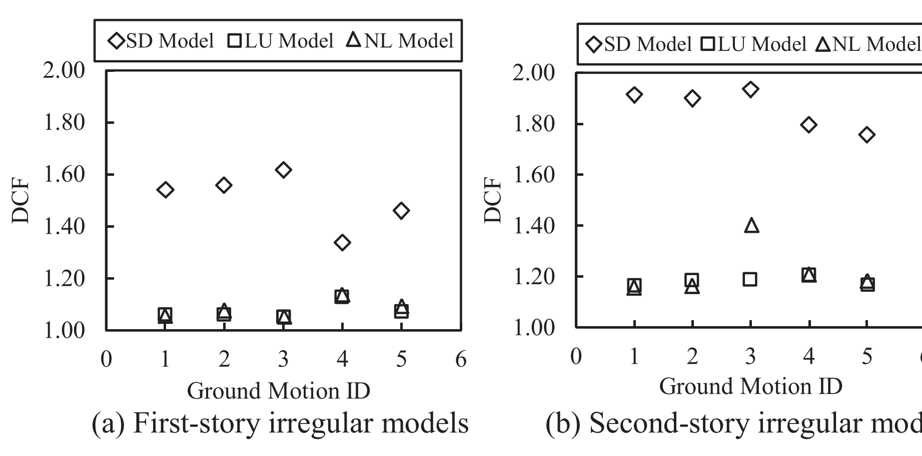

Fig. 18. Drift concentration factors (DCFs) of irregular models.

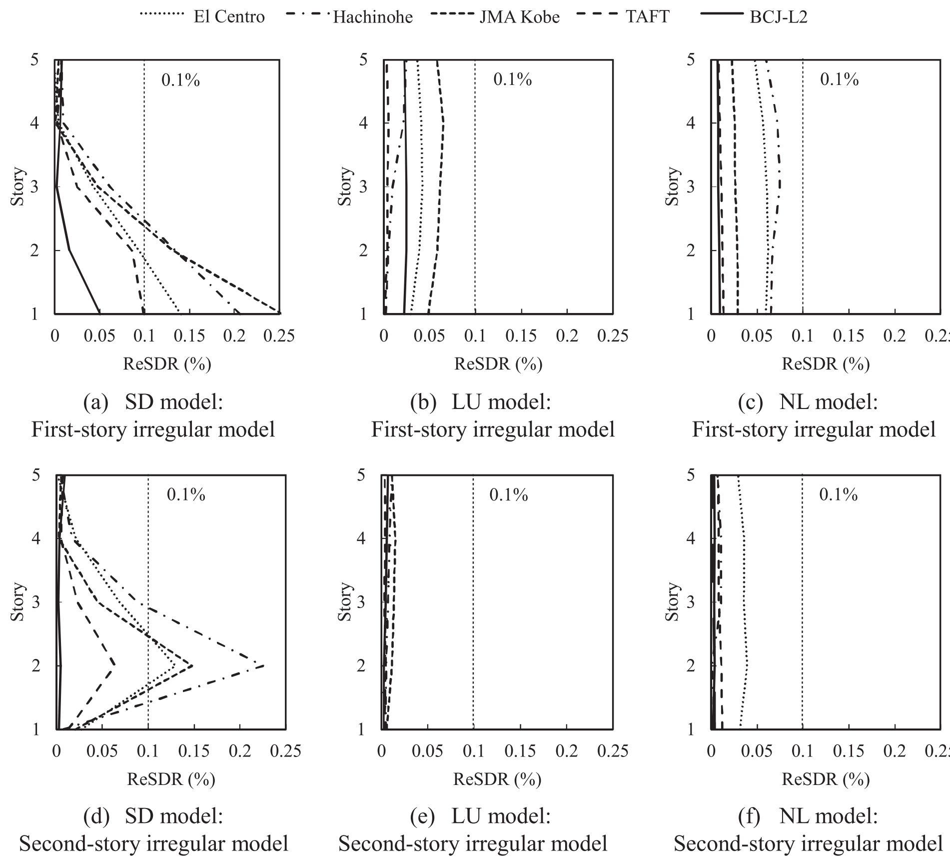

Fig. 19. Residual story drift ratio (ReSDR) of each story in irregular models.

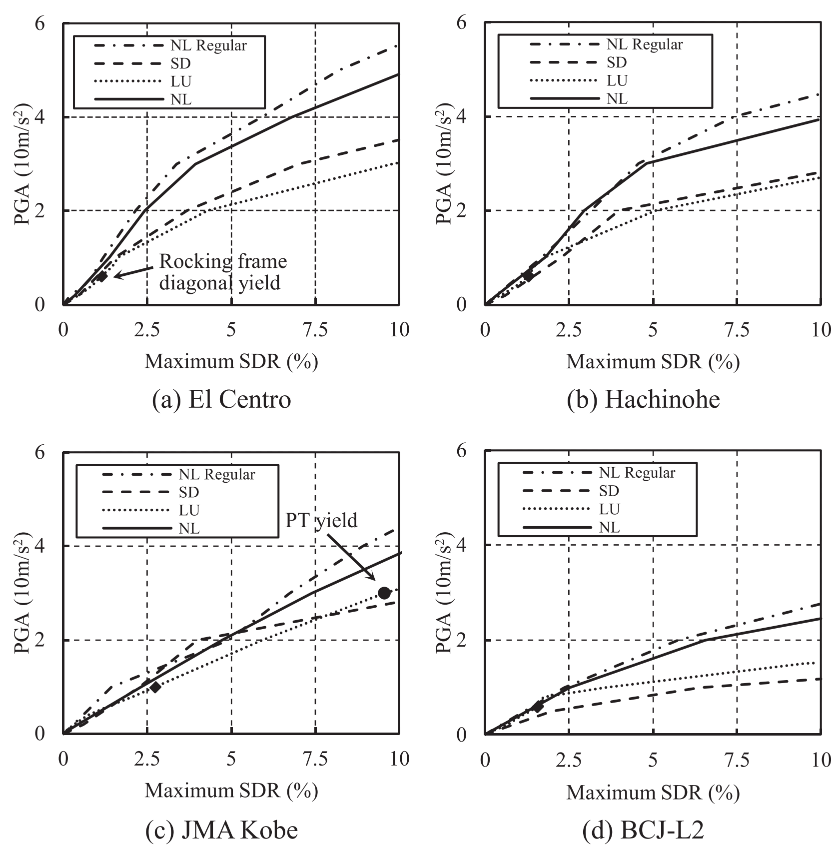

Fig. 20. Incremental dynamic analysis curves of first-story irregular models.

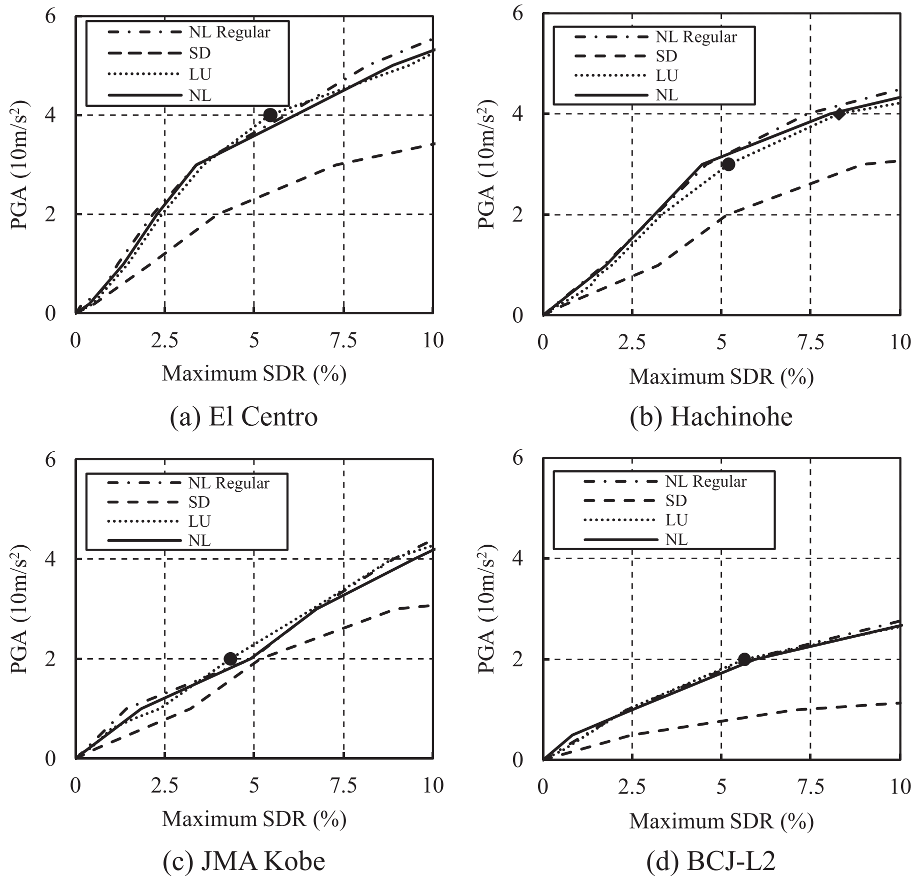

Fig. 21. Incremental dynamic analysis curves of second-story irregular models.

model achieved the smallest SDR and DCF compared with the SD and LU models. Additionally, the ReSDR of the NL model was as small as that of the LU model, even without PT strands. In terms of energy dissipation, the LU model resulted in more damage in the envelope frames, whereas in the proposed NL model, the envelope frames remained almost undamaged.

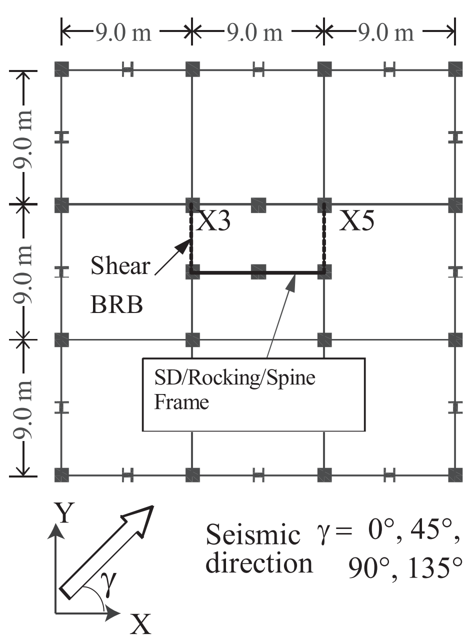

Fig. 22. Modified model which employed hybrid systems.

(2) In the IDA analysis of regular models, both the LU model and the NL model showed stable seismic performance with increased input ground motion intensity, regardless of the yielding of the PT strands in the LU model.
(3) For the irregular models with unbalanced vertical strength distributions subjected to a design-level earthquake, the SDR, DCF, and ReSDR of the LU and NL models were consistent with those of the regular models. In contrast, severe damage concentration in the irregular story was observed in the SD model.
(4) The first-story irregular LU model exhibited degradation after the bottom diagonal members in the rocking frame yielded during IDA analysis, similar to the degradation of the SD model. In contrast, the proposed NL model showed stable performance with increased input ground motion intensity even with the irregular first story.
(5) For the structures with the NL system in one plan direction and the SD system in the other direction, its behavior against bi-directional ground motions cannot be simply evaluated by superposing the behaviors in each direction, as the interaction between the BRBs and the spine frame is significant. The participation of BRBs (SD-dir.) in dissipating earthquake energy increases with the input angle from NL-dir. increasing.

In summary, NL spine frame was verified as showing excellent performance in preventing damage concentration in weak stories as well as sufficient self-centering capacity and robustness under large earthquakes even without PT strands. The proposed system is currently being employed in the design of an actual building, the construction of which started in March 2014. The detail at the base of the spine frame is shown in Fig. 24. The building is completed in 2015. The construction

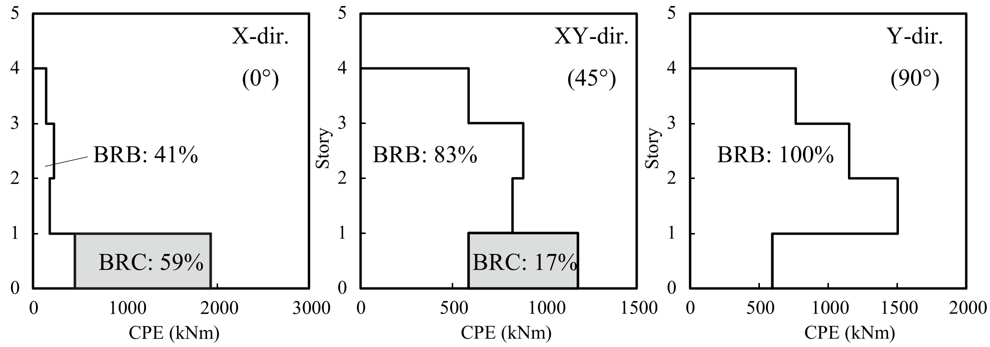

Fig. 23. Cumulative strain energy dissipated by BRCs and BRBs.

process and studies of the simple design method of this structural system will be reported in the near future.

Abbreviations and notations

SD	conventional frame with shear dampers as BRBs
LU	uplifting rocking frame
NL	non-uplifting spine frame
SMRF	steel moment-resisting frame
BRC	buckling-restrained column member
BRB	buckling-restrained brace
BRBF	buckling-restrained braced frame
RDR	roof drift ratio
SDR	story drift ratio
PT	post-tensioned
DCF	story drift concentration factor (maximum SDR:RDR ratio)
ReSDR	residual story drift ratio
CPE	cumulative plastic strain energy
Z	seismic zones coefficient
A_i	distribution factor of seismic load along the structure height
R_t	seismic response reducing factor
C_0	standard shear coefficient
D_{si}	structure characteristic coefficient
F_{esi}	shape factor
F_s	eccentricity factor
F_e	stiffness factor
M_{OT}	overturning moment

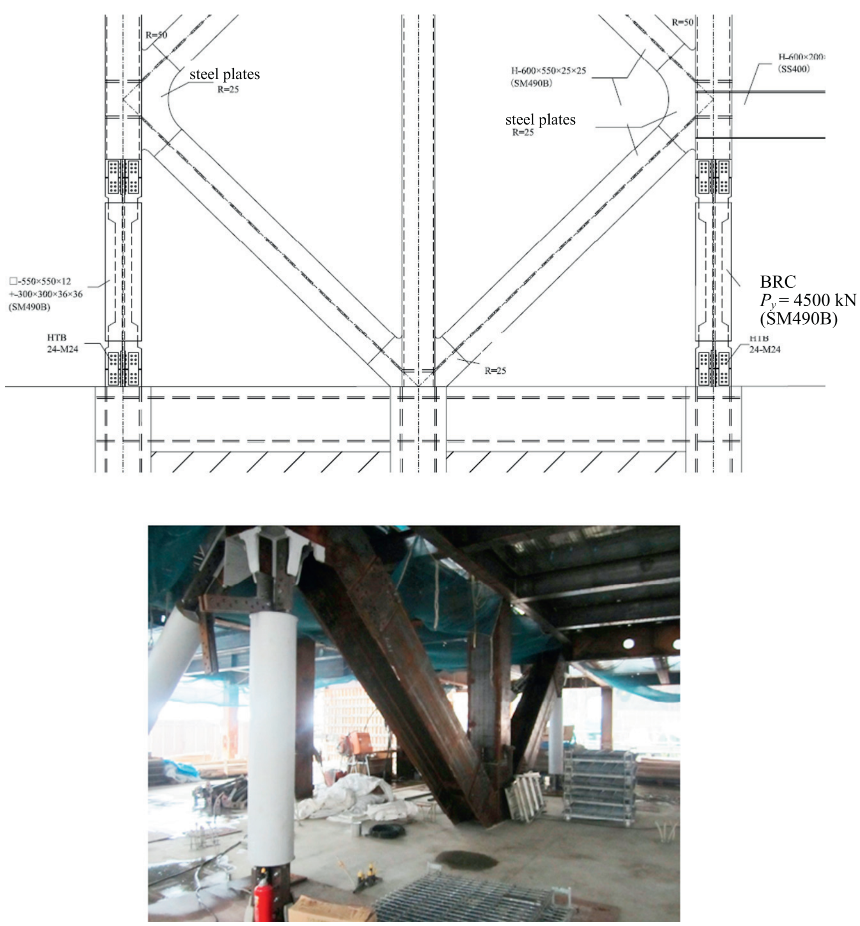

Fig. 24. Detail of the base of the NL spine frame.

G_{rf} gravity load on the rocking frame
F_{PT} axial force of PT wire
F_y^{BRC} yielding force of BRC
b_{rf} width of rocking frame

Appendix A

A.1. Design procedure for the prototype building based on Japanese seismic code

Based on Japanese seismic code, the seismic performance of a seismic resisting building should be verified at two limit states: (1) damage initiation state and (2) life-safety limit state. These states correspond to a hazard of 63.6% and 10% probability of exceedance in a 50-year period (DBE level). The prototype building was designed by static analysis with equivalent static horizontal load for each seismic level. For level 1 seismic design, the equivalent loads are calculated by Eqs. (A-1) to (A-3). All of the structure members remain elastic and the maximum story drift ratio is less than 0.5%.

$$Q_i = C_0 \cdot Z \cdot R_t \cdot A_i \cdot \sum_{j=1}^{N} w_j \quad (\text{A}-1)$$

$$A_i = 1 + \left(\frac{1}{\sqrt{\alpha_i}} - \alpha_i\right)\frac{2T}{1+3T} \quad \alpha_i = \frac{\Sigma W_i}{W} \quad (\text{A}-2)$$

$$R_t = 1 - 0.2\left(\frac{T}{T_c} - 1\right)^2 = 0.724 \quad (\text{A}-3)$$

where, Z is the coefficient representing different seismic zones. A_i is the distribution factor of seismic load along the structure height related with the fundamental period. R_t is the reducing factor considering the vibration characteristics of foundation and buildings. C_0 is the standard shear coefficient (Lv.1 design $C_0 = 0.2$, Lv.2 design $C_0 = 1.0$). w_i is the weight of each story.

For the level 2 seismic design, the necessary equivalent loads are calculated by Eq. (A-4). It is less than the load bearing capacity. The load bearing capacity is the horizontal load when the maximum story drift ratio reached 1.0% in pushover analysis, where the story horizontal loads are in proportion with A_i distribution.

$$Q_{uni} = D_{si} F_{esi} Z R_t A_i C_0 \sum_{i=1}^{n} wi \quad (\text{A}-4)$$

where, D_{si} takes account of structural damping ratio and ductility, which is 0.25 for this structure. F_{esi} is the shape factor, which is the product of the eccentricity factor F_s and the stiffness factor F_e, all of the three parameters are 1.0 here.

The seismic performance of the envelope steel frame in the prototype building has been verified by the above design method. In level 2 seismic design, the maximum story drift ratio of the envelop frame is 0.43%, less than 1.0%. Besides, the ratio of the shear force capacity and necessary story shear force is 2.342, exhibiting high safety. Therefore even for the level 2 seismic input, we can expect that the envelope structural framework remains elastic and most of the input seismic energy is absorbed by the energy-dissipation members.

Appendix B

B.1. Analytical modeling of BRBs/BRCs

In the modeling of BRBs/BRCs, we adopted equivalent elastic modulus and equivalent strain hardening ratio in order to consider that contribution of the higher axial stiffness of the elastic portions of the same member. The two equivalent parameters are calculated by Eqs. (B-1) and (B-2).

$$E_{eq} = E\frac{l_c + l_e}{l_c + l_e\dfrac{A_c}{A_e}} \quad (\text{when BRBs (BRCs) are elastic}) \quad (\text{B}-1)$$

$$\frac{E_{heq}}{E_{eq}} = \frac{E_h}{E}\frac{l_c + l_e\dfrac{A_c}{A_e}}{l_c + l_e\dfrac{A_c}{A_e}\dfrac{E_h}{E}} \quad (\text{after BRBs (BRCs) yield}) \quad (\text{B}-2)$$

where, l_c and A_c is the length and area of the core portion. l_e and A_e is the length and area of the elastic portions. E_h is the tangent modulus of core steel after yielding.

References

[1] P. Uriz, S.A. Mahin, Toward earthquake-resistant design of concentrically braced steel-frame structures, PEER-2008/08, Pacific Earthquake Engineering Research Center (PEER), University of California, Berkeley, 2008.
[2] M.M. Garlock, R. Sause, J.M. Ricles, Behavior and design of posttensioned steel frame systems, J. Struct. Eng. 133 (3) (2007) 389–399, http://dx.doi.org/10.1061/(ASCE)0733-9445.
[3] D.J. Miller, L.A. Fahnestock, M.R. Eatherton, Development and experimental validation of a nickel–titanium shape memory alloy self-centering buckling-restrained brace, Eng. Struct. 40 (2012) 288–298, http://dx.doi.org/10.1016/j.engstruct.2012.02.037.
[4] C. Christopoulos, R. Tremblay, H.-J. Kim, M. Lacerte, Self-centering energy dissipative bracing system for the seismic resistance of structures: development and validation, J. Struct. Eng. 134 (2008) 96–107, http://dx.doi.org/10.1061/(ASCE)0733-9445(2008)134:1(96) (SPECIAL ISSUE: Design and Analysis of Structures with Seismic Damping Systems).
[5] M. Midorigawa, T. Azuhata, T. Ishihara, Y. Matsuba, Y. Matsushima, A. Wada, Earthquake response reduction of buildings by rocking structural system, Smart Structures and Materials 2002: Smart Systems for Bridges, Structures, and Highways; Proceedings of SPIE, 4696 2002, pp. 265–272.
[6] T. Takeuchi, M. Midorikawa, K. Kasai, G. Deierlein, X. Ma, J.F. Hajjar, T. Hikino, Shaking table test of controlled rocking frames using multipurpose test bed, The Sixth European Conference on Steel and Composite Structures, Budapest, Hungary, 2011.
[7] A. Wada, S. Yamada, O. Fukuta, M. Tanigawa, Passive controlled slender structures having special devices at column connections, Seventh International Seminar on Seismic Isolation, Passive Energy Dissipation and Active Control of Vibrations of Structures, Assisi, Italy, 2001.
[8] R. Tremblay, L.P. Poirier, N. Bouaanani, M. Leclerc, V. Rene, L. Fronteddu, S. Rivest, Innovative viscously damped rocking braced steel frames, Proceedings of the 14th World Conference on Earthquake Engineering, Beijing, China, Paper No. 05-01-0527, 2008.
[9] G.W. Housner, The behavior of inverted pendulum structures during earthquakes, Bull. Seismol. Soc. Am. 53 (2) (1963) 403–417.
[10] R.W. Clough, A.A. Huckelbridge, Preliminary experimental study of seismic uplift of a steel frame, Report No. UCB/EERC-77/22, Earthquake Engineering Research Center (EERC), 1977.
[11] M.J.N. Priestley, R.J. Evison, A.J. Carr, Seismic response of structures free to rock on their foundations, Bull. N. Z. Natl. Soc. Earthq. Eng. 11 (3) (1978) 141–150.
[12] Z. Qu, A. Wada, S. Motoyui, H. Sakata, S. Kishiki, Pin-supported walls for enhancing the seismic performance of building structures, Earthq. Eng. Struct. Dyn. 41 (2012) 2075–2091, http://dx.doi.org/10.1002/eqe.2175.
[13] B. Janhunen, S. Tipping, J. Wolfe, T. Mar, Seismic retrofit of a 1960s steel moment-frame highrise using a pivoting spine, Proceedings of the Structural Engineers Association of California 82nd Annual Convention, San Diego, USA, 2013.
[14] S. Günay, M. Korolyk, D. Mar, K. Mosalam, J. Rodgers, Infill walls as a spine to enhance the seismic performance of non-ductile reinforced concrete frames, Improving the Seismic Performance of Existing Buildings and Other Structures 2009, pp. 1093–1104, http://dx.doi.org/10.1061/41084(364)100.
[15] M. Eatherton, J. Hajjar, X. Ma, H. Krawinkler, G. Deierlein, Seismic design and behavior of steel frames with controlled rocking—part I: concepts and quasi-static subassembly testing, The 2010 NASCC & Structures Congress, Orlando, USA 2010, pp. 1523–1533, http://dx.doi.org/10.1061/41130(369)138.
[16] M.R. Eatherton, J.F. Hajjar, Residual drifts of self-centering systems including effects of ambient building resistance, Earthquake Spectra 27 (3) (2011) 19–774, http://dx.doi.org/10.1193/1.3605318.
[17] X. Ma, M. Eatherton, J. Hajjar, H. Krawinkler, G. Deierlein, Seismic design and behavior of steel frames with controlled rocking—part II: large scale shake table testing and system collapse analysis, The 2010 NASCC & Structures Congress, Orlando, USA 2010, pp. 1534–1543, http://dx.doi.org/10.1061/41130(369)139.
[18] G. Deierlein, X. Ma, M. Eatherton, J. Hajjar, H. Krawinkler, T. Takeuchi, K. Kasai, Midorikawa M. Earthquake resilient steel braced frames with controlled rocking and energy dissipating fuses, The Sixth European Conference on Steel and Composite Structures, Budapest, Hungary, 2011.

[19] M. Midorikawa, T. Azuhata, T. Ishihara, A. Wada, Shaking table tests on seismic response of steel braced frames with column uplift, Earthq. Eng. Struct. Dyn. 35 (2006) 1767–1785, http://dx.doi.org/10.1002/eqe.603.
[20] M. Ikenaga, T. Nagae, M. Nakashima, K. Suita, Development of column bases having self-centering and damping capability, Proceedings of the Fifth International Conference on Behaviour of Steel Structures in Seismic Areas, STESSA, Yokohama, Japan 2006, pp. 703–708.
[21] T. Takamatsu, H. Tamai, T. Yamanishi, A. Matsuo, Rehabilitation of steel structure by means of wedge device, Proceedings of the 14th World Conference on Earthquake Engineering, Beijing, China, 2008.
[22] T. Takeuchi, K. Suzuki, Performance-based design for truss–frame structures using energy dissipation devices, Proceedings of the Fourth International Conference on Behaviour of Steel Structures in Seismic Areas, STESSA, Naples, Italy 2003, pp. 55–62.
[23] S. Mazzoni, F. McKenna, M.H. Scott, G.L. Fenves, OpenSEES Version 2.0 User Manual, Pacific Earthquake Engineering Research Center (PEER), University of California, Berkeley, 2009. (Available from: http://opensees.berkeley.edu, last accessed March 2014).
[24] FEMA-355, State of the Art Report on Performance Prediction and Evaluation of Steel Moment-frame Buildings, Earthquake Engineering Research Institute for the Federal Emergency Management Agency (FEMA), Washington, D.C., 2000
[25] D. Vamvatsikos, C.A. Cornell, Incremental dynamic analysis, Earthq. Eng. Struct. Dyn. 31 (3) (2002) 491–514, http://dx.doi.org/10.1002/eqe.141.
[26] A.A.K. Al-Ali, H. Krawinkler, Effects of Vertical Irregularities on Seismic Behavior of Building Structures, Report No. 130, The John A. Blume Earthquake Engineering Center, Department of Civil and Environmental Engineering, Stanford University, Stanford, USA, 1998.
[27] C. Chintanapakdee, A.K. Chopra, Seismic response of vertically irregular frames: response history and modal pushover analyses, J. Struct. Eng. 130 (8) (2004) 1177–1185, http://dx.doi.org/10.1061/(ASCE)0733-9445(2004)130:8(1177).